RESEARCH ARTICLE | OCTOBER 26 2022

The phase-2 particle x-ray temporal diagnostic for simultaneous measurement of multiple x-ray and nuclear emission histories from OMEGA implosions (invited)

N. Kabadi ✉ 📵 ; P. Adrian 📵 ; C. Stoeckl 📵 ; A. Sorce; H. W. Sio 📵 ; M. Bedzyk; T. Evans 📵 ; S. Ivancic 📵 ;
J. Katz 📵 ; J. Knauer; J. Pearcy 📵 ; D. Weiner; R. Betti; A. Birkel 📵 ; D. Cao; M. Gatu Johnson 📵 ;
S. P. Regan 📵 ; R. D. Petrasso 📵 ; J. Frenje 📵

Check for updates

View Online   Export Citation   CrossMark

The phase-2 particle x-ray temporal diagnostic for simultaneous measurement of multiple x-ray and nuclear emission histories from OMEGA implosions (invited)

View Online   Export Citation   CrossMark

N. Kabadi,[1,a] P. Adrian,[1] C. Stoeckl,[2] A. Sorce,[2] H. W. Sio,[3] M. Bedzyk,[2] T. Evans,[2] S. Ivancic,[2] J. Katz,[2] J. Knauer,[2] J. Pearcy,[1] D. Weiner,[2] R. Betti,[2] A. Birkel,[1] D. Cao,[2] M. Gatu Johnson,[1] S. P. Regan,[2] R. D. Petrasso,[1] and J. Frenje[1]

AFFILIATIONS

[1] Massachusetts Institute of Technology Plasma Science and Fusion Center, Cambridge, Massachusetts 02139, USA
[2] University of Rochester Laboratory for Laser Energetics, Rochester, New York 14623, USA
[3] Lawrence Livermore National Laboratory, Livermore, California 94550, USA

Note: This paper is part of the Special Topic on Proceedings of the 24th Topical Conference on High-Temperature Plasma Diagnostics.
[a] Author to whom correspondence should be addressed: kabadi@mit.edu

ABSTRACT

Electron-temperature (T_e) measurements in implosions provide valuable diagnostic information, as T_e is negligibly affected by residual flows and other non-thermal effects unlike ion-temperature inferred from a fusion product spectrum. In OMEGA cryogenic implosions, measurement of $T_e(t)$ can be used to investigate effects related to time-resolved hot-spot energy balance. The newly implemented phase-2 Particle X-ray Temporal Diagnostic (PXTD) utilizes four fast-rise (~15 ps) scintillator-channels with distinct x-ray filtering. Titanium and stepped aluminum filtering were chosen to maximize detector sensitivity in the 10–20 keV range, as it has been shown that these x rays have similar density and temperature weighting to the emitted deuterium–tritium fusion neutrons (DTn) from OMEGA Cryo-DT implosions. High quality data have been collected from warm implosions at OMEGA. These data have been used to infer spatially integrated $T_e(t)$ with <10% uncertainty at peak emission. Nuclear and x-ray emission histories are measured with 10 ps relative timing uncertainty for x rays and DTn and 12 ps for x rays and deuterium-^{3}He protons (D^{3}Hep). A future upgrade to the system will enable spatially integrated $T_e(t)$ with 40 ps time-resolution from cryogenic DT implosions.

I. BACKGROUND AND MOTIVATION

The goal of an inertial confinement fusion (ICF) experiment is to spherically compress deuterium and tritium (D and T) fuel to reach the high temperatures and densities necessary to achieve a burning plasma state. An imploding DT fuel-shell is accelerated to high velocity. The shell kinetic energy is transferred to the thermal energy of the central DT plasma (hot-spot) as the shell is converging, increasing the hot-spot density and temperature.[1,2] To reach ignition, this compression must happen symmetrically, efficiently transferring energy from the shell to the hot-spot. The details of this energy transfer and the overall hot-spot energy balance must be understood to push toward robust fusion-ignition designs.

The current understanding of hot-spot thermal energy relies heavily on temporally and spatially averaged ion temperatures inferred from the widths of fusion product spectra, primarily the spectra of deuterium–tritium neutrons (DTn) and deuterium–deuterium neutrons (DDn).[3] These measurements do provide valuable information but are not solely dependent on the hot-spot ion temperature (T_i) as residual flows often substantially broaden the

measured spectra and increase the apparent T_i.[4–7] In contrast, electron temperatures (T_e) inferred from the shape of the emitted x-ray spectrum are practically unaffected by residual kinetic energy in ICF implosions. This is because the electron thermal velocity is significantly larger than any bulk plasma flow. For this reason, measured T_e provides valuable information about the thermal energy of the hot-spot, which will be used to investigate hot-spot energy balance, impacts of residual kinetic energy, ion-electron equilibration, and compression efficiency. In the Cryo-DT implosions conducted at the Omega laser facility, the electrons and ions are not thermally equilibrated during peak compression.[8] This makes a time-resolved T_e measurement critical for understanding hot-spot energy balance.

The focus of this work is the implementation and initial use of a fast-rise-scintillator-based diagnostic capable of simultaneously capturing multiple x-ray and nuclear emission histories at OMEGA. This diagnostic is referred to as the phase-2 Particle X-ray Temporal Diagnostic (PXTD) as it is a new upgraded version of the existing phase-1 PXTD.[9] Phase-2 PXTD measured x-ray emission histories are used to infer the time-resolved electron temperature [$T_e(t)$] with 40 ps time resolution and 10% uncertainty at peak emission. Simultaneous x-ray and nuclear emission histories have been captured and compared with 10 ps relative timing uncertainty. The subsequent sections discuss the diagnostic principle, initial results from using the instrument on warm implosions, and planned upgrades to collect high-quality data from Cryo-DT implosions at OMEGA.

II. DIAGNOSTIC DESIGN

The phase-1 and phase-2 PXTD diagnostics both utilize 1-mm thick commercially available BC-422 scintillators. For the phase-2 system, these scintillators are positioned between 6 and 10 cm from the target chamber center (TCC) within a dedicated nosecone. The distance to TCC can be selected based on the expected nuclear and x-ray yields. A cut-away view of the phase-2 nosecone is shown in Fig. 1. Each scintillator is independently filtered. The filtering is selected to measure nuclear products and/or x rays in different energy bands. Examples of different filter setups and the recorded signals are discussed in Secs. III and IV. After passing through the filters, the nuclear products and/or x rays deposit energy in the scintillators, which subsequently emit ultraviolet (UV) light with a characteristic time-history. The emitted scintillator light is relayed to an optical streak camera that is located in a shielded location. The optical relay and streak camera are identical to the components used by the neutron temporal diagnostic (NTD).[10]

The scintillator emission history rises at ~15 ps and decays over ~1.2 ns.[11] The fast rise and slow decay mean that all of the nuclear and x-ray history information is encoded in the rising edge of the recorded signal.

There are three key distinguishing features that make phase-2 PXTD an improved system:

- The streak camera is located in a shielded location.
- Improved UV and electron optics.
- Decreased temporal blurring.

These advantages come from using the optical relay and camera from the NTD, and descriptions of them can be found in Ref. 10. With the streak camera located in a shielded location, high quality
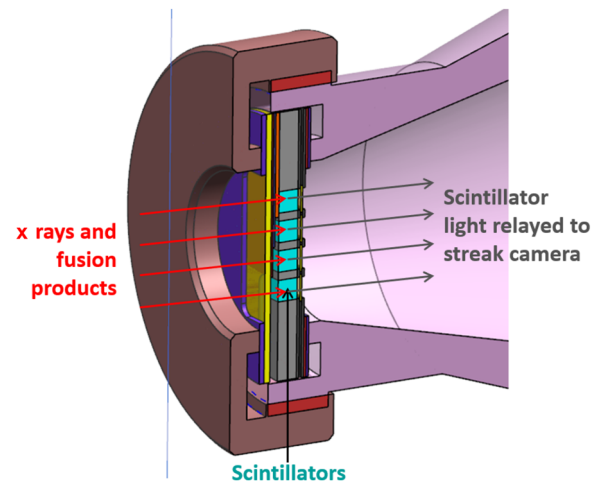

FIG. 1. A cut away view of the four-scintillator-channel nosecone design used for phase-2 PXTD. Each channel has differential filtering to measure nuclear products and/or x rays in different energy bands. The scintillators can be positioned between 6 and 10 cm from the target chamber center (TCC).

data are collected on high yield DT implosions, which was not possible with the phase-1 system. The improved UV optics in the light relay and electron optics within the modern streak camera decrease the spatial blurring in the vertical (non-temporal) direction, allowing for more channels. The streak camera is a Rochester Optical Streak System (ROSS).[12] Examples of streak images collected with the phase-1 and phase-2 PXTD are shown in Figs. 2(a) and 2(b). It is clear that the phase-2 PXTD streak image is significantly sharper with distinct separation between the four channels. Based on these data, it is possible to fabricate a new nosecone assembly with five independent channels, greatly improving upon the original three-channel maximum of phase-1 PXTD. Additional channels are used to sample additional x-ray bands to improve $T_e(t)$ measurement accuracy or to measure additional nuclear products simultaneously. A previous study showed that five channels provide an optimal balance of signal statistics in each channel and spectral coverage.[13] Decreased temporal blurring is achieved with the same improved optics and a modern streak camera. The rising edge of the impulse response function (IRF) for the phase-1 and phase-2 PXTD is shown in Fig. 2(c). Phase-1 PXTD has a characteristic rise time of 126 ps while phase-2 is 40 ps as measured using short x-ray pulses driven using an OMEGA-EP beam.[10] The IRF is assumed to be constant for all scintillators used, and further work is necessary to verify this assumption. This improvement is critical as typical ICF x-ray and nuclear emission histories are ~100 ps FWHM. Phase-2 PXTD is capable of providing significantly more information about the emission history shape compared to phase-1.

To infer the emission histories from the streak images recorded with phase-2 PXTD, the following steps are used:

- A median filter is applied in the vertical direction.
- The fiducial and comb pulses are used to establish the temporal axis.
- The signal in each channel is isolated and summed in the vertical direction.
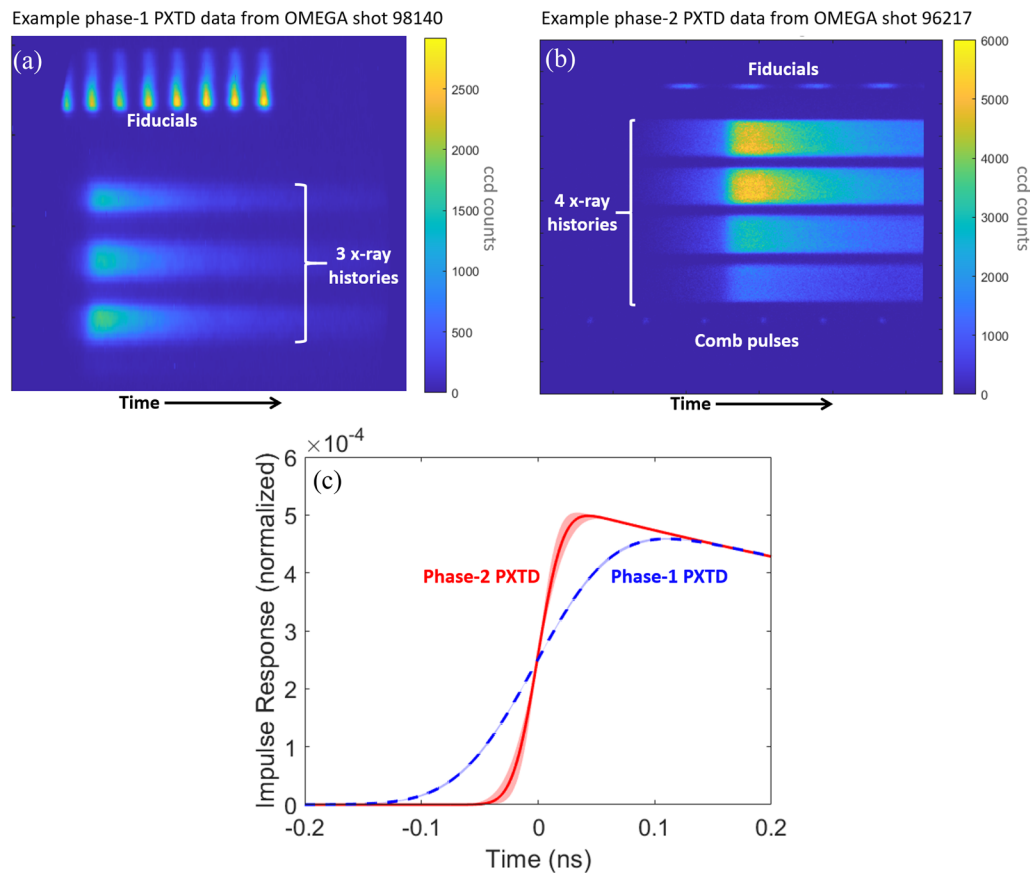
Example phase-1 PXTD data from OMEGA shot 98140

Example phase-2 PXTD data from OMEGA shot 96217

FIG. 2. (a) Streak image with three x-ray emission histories collected with the phase-1 PXTD. (b) Streak image with four x-ray emission histories collected with the phase-2 PXTD. (c) The rising edge of the integral normalized temporal impulse response of the phase-1 and phase-2 PXTDs, indicating that the phase-2 PXTD has a significantly faster response (about 3× faster) than phase-1 PXTD. When contrasting the streak images in (a) and (b), it is clear that the phase-2 PXTD streak image is sharper, allowing for more scintillator channels to be used. The fiducial pulses labeled (a) and (b) are used for absolute timing relative to the laser pulse, and the comb pulses in B are used to accurately determine the relative time-axis.

- The impulse response and Doppler broadening are deconvolved.
- The emission histories are corrected for time-of-flight to the scintillators.

The median filter is applied to remove any single pixel background from direct DTn interacting with the CCD. It is applied in the vertical direction to avoid impacting the system's temporal response. The fiducial and comb pulses are seen in Fig. 2(b). The fiducials have known absolute timing relative to the laser pulse and fixed spacing of 0.548 ns. The comb pulses are not absolutely timed but have a fixed spacing of 0.5 ns in Fig. 2(b). Since these data were collected, a higher-frequency comb with 0.2 ns spacing has been implemented. An absolute time-axis is established by fitting a cubic polynomial to the combination of fiducial and comb pulse locations. Given the high linearity of the streak, a cubic polynomial is sufficient to constrain the time axis. After vertically summing the signal in each channel, CCD counts are converted to the number of photo-electrons to determine the counting statistics. The number of photo-electrons is used as there are fewer photo-electrons

generated within the streak camera than input photons, and the conversion to CCD counts is a gain process. The conversion factor used is 150 CCD counts per photo-electron based on previous experiments with similar streak cameras.[14] From the signal in each channel, the impulse response (and Doppler broadening for nuclear products) is deconvolved to determine the emission history. The deconvolution is conducted using a least-squares error minimization of a modified Akima interpolant.[15] The statistical-uncertainty analysis is conducted using the method of Lerche outlined in Ref. 16. Finally, the signals are corrected for their different times-of-flight from TCC to the scintillators.

One of the most powerful aspects of PXTD is the ability to simultaneously capture multiple emission histories on a single streak image. This enables comparison of the histories without the need for cross timing different instruments, avoiding additional uncertainty due to fiducial jitter (~30 ps on OMEGA). When comparing multiple histories measured on a single streak, the primary sources of uncertainty come from time-of-flight, streak linearity, and statistics. A summary of the timing uncertainty when comparing recorded x-rays and relevant nuclear-product histories is shown in Table I. The top

TABLE I. Timing uncertainties when contrasting two different emission histories collected on a single streak with phase-2 PXTD. (Top) Systematic uncertainties due to time-of-flight and streak-sweep non-linearity. (Bottom) Minimum uncertainty with optimal statistics. The statistical uncertainty is limited by the maximum throughput of the streak camera. The tables are read by looking at the intersection of the row and column associated with the two emissions to be contrasted.

	DTn	D³Hep	DDn
Uncertainties due to time-of-flight and streak linearity			
X rays	7 ps	9 ps	22 ps
DTn		9 ps	22 ps
D³Hep			23 ps
Optimal uncertainties including statistical contributions			
X rays	10 ps	11 ps	23 ps
DTn		11 ps	23 ps
D³Hep			24 ps

section shows the uncertainty due to time-of-flight and streak linearity, while the bottom includes the statistical contribution, assuming optimal performance. The best-case statistics are limited by the maximum through-put of the streak camera. When comparing x rays, DTn, and D³Hep signals, uncertainties of 10–11 ps, are achieved, while for DDn, the uncertainty is 23–24 ps due to their lower mean energy and longer time-of-flight.

III. MEASUREMENT OF SPATIALLY INTEGRATED $T_e(t)$

By recording multiple x-ray emission histories in different energy bands, information about the time resolved x-ray spectrum is captured and used to infer $T_e(t)$. The x-ray emission from an ICF hot-spot is dominated by bremsstrahlung, which has a characteristic shape given by

$$S(E) \propto e^{-E/T_e}, \qquad (1)$$

where $S(E)$ is the emitted spectrum and E is the x-ray energy in keV. From this expression, it is clear that the spectral shape is determined
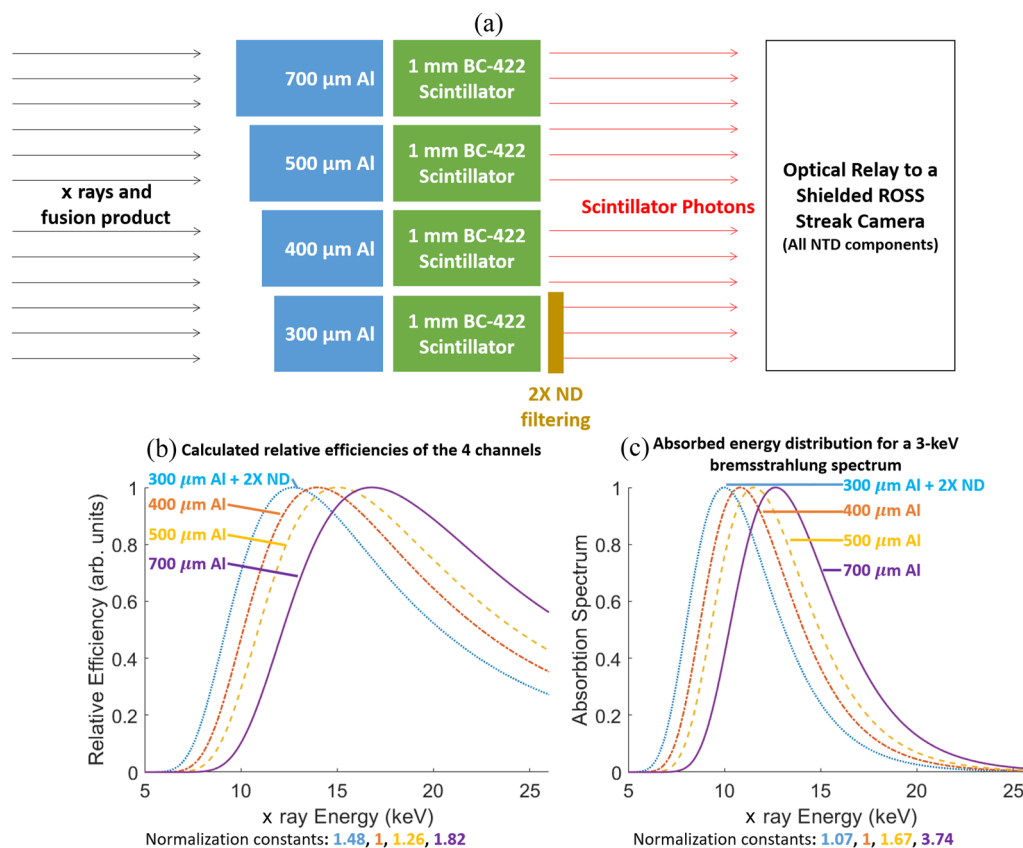

FIG. 3. (a) Schematic of the phase-2 PXTD filter setup used for measurement of $T_e(t)$. Each channel is filtered with a different thickness of aluminum to measure x rays in different energy bands. The scintillator output for the softest filtered channel is reduced by 2× with a neutral-density (ND) filter. (b) Peak normalized relative efficiencies for the four channels shown in (a). (c) The spectra of x rays absorbed within the scintillators for an incident 3 keV bremsstrahlung spectrum. The relative normalization constants used for each channel are shown below the figures in (b) and (c). The energy range coverage of the four channels is sufficient to infer the shape of the incident x-ray spectrum and $T_e(t)$.

entirely by T_e. $T_e(t)$ is, therefore, inferred from the relative amplitudes of the multiple x-ray emission histories within each time bin. This is done by using a forward model and a synthetic diagnostic as discussed in Ref. 13. For this analysis, the filters' x-ray transmissions are measured using the setup described in Ref. 17, and the scintillator UV conversion efficiency as a function of x-ray energy is assumed to be constant. Future experiments are planned to measure the scintillator conversion efficiency.

Figure 3(a) shows the filter setup used for the measurement of $T_e(t)$. Four scintillator-channels were used with 300, 400, 500, and 700 μm Al x-ray filters. Behind the 300 μm Al channel, an ND filter is used to reduce the scintillator emission by 2× to capture all four signals with high statistics within the dynamic range of the streak camera. As shown in Figs. 3(b) and 3(c), each channel is sensitive to a different x-ray energy band. The peaks of spectra of x rays absorbed by the scintillators occur in the range of 10–13 keV for a 3 keV bremsstrahlung spectrum. High-quality data in all four channels were collected using this configuration on OMEGA D³He gas-filled shock-driven implosion 96 217 as shown in Fig. 4. In Fig. 4(b), the results of inferring $T_e(t)$ from the histories are shown in the black points, while the total x-ray emission history, determined by summing the raw x-ray signals before deconvolution, is shown in blue. The $T_e(t)$ inferred from phase-2 PXTD agrees with other measurements of the emission averaged T_e, like from the x-ray-imaging spectrometer,[18] and is significantly lower than the ion temperature inferred from the width of the DDn spectrum.[3] This is expected for this type of shock-driven implosion where the ions are shock-heated to high temperature, and the ion–electron equilibration time is long compared to the dynamic time-scale. The electron temperature is constant as a function of time, within the error bars, which is consistent with the expectation for this implosion type. Error bars on the electron temperature include contributions from random statistics, signal to noise, and calibration uncertainty as discussed in Ref. 13. An additional strength of this diagnostic is observed in Fig. 4(b) where the early time coronal or laser plasma interaction (LPI) x-ray emission is distinguished in time from the core emission. An emission averaged diagnostic would not be able to separate these two sources.

IV. SIMULTANEOUS X-RAY AND NUCLEAR EMISSION HISTORIES

Simultaneous x-ray and DTn histories were captured using the phase-2 PXTD on a series of warm plastic (CH) shell implosions conducted at OMEGA. These experiments are Cryo-DT-implosion surrogates using a CH ablator that is mass equivalent to the ablator and DT-ice in a Cryo capsule. These implosions are driven with a laser pulse identical to what is used in Cryo-DT experiments. The filter setup used is similar to what is shown in Fig. 3(a), with 100 μm Ti filtering added to all channels, the 700 μm Al filter replaced with 1 mm of W, and the 2× ND filter removed. The 1-mm W filter is used for a dedicated DTn channel as it blocks practically all incident x rays. The additional 100 μm Ti filter was added to suppress low energy non-hotspot x-ray emission that was present in initial tests on Cryo-DT implosions. A full discussion of this can be found in Ref. 13. With this filtering configuration, the channels are all sensitive to a similar x-ray energy range, making an inference of $T_e(t)$ impossible. Figure 5(a) shows a phase-2 PXTD streak image collected on the warm Cryo surrogate shot 100 521. The three x rays and four DTn signals are summed, and then, the IRF is deconvolved to determine emission histories shown in Fig. 5(b). In the case of the DTn signals, the shape of the raw signal near the peak is different for the 1 mm W channel as compared to the other three. The cause of this difference is not known and warrants further investigation. The deviation occurs after the majority of the signal rises and, therefore, only affects the late tail of the inferred history and not the peak location or FWHM. From the two histories, the time of peak x-ray emission (x-ray bang time) is determined to be 3 ± 10 ps after the time of peak DTn emission (nuclear bang time). Simulations of this experiment performed with the 1D hydrodynamic code standardly used for implosion design at OMEGA, LILAC,[19] and predicted that the x-ray bang time should be delayed by 20 ps relative to the nuclear bang time, which is outside the measured uncertainty range. This indicates that 1D hydrodynamic simulations are not capturing the detailed dynamics of the ICF hot-spot during emission.

The phase-2 PXTD has also been used to simultaneously capture the x-ray and D³Hep emission histories on a series of D³He
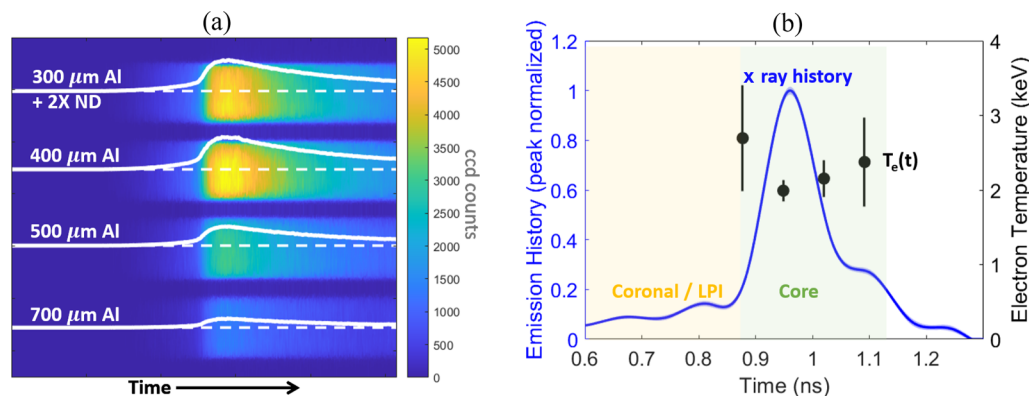
FIG. 4. (a) Phase-2 PXTD measured streak image for OMEGA D³He gas-filled shock-driven implosion 96217. (b) The deconvolved x-ray emission history (blue) with a shaded 95% confidence interval determined by summing the four signals in (a) and then deconvolving the impulse response function (IRF) and $T_e(t)$ (black points) inferred with 40 ps time resolution and 10% uncertainty at peak emission. A diagram of the imploded capsule is also shown.
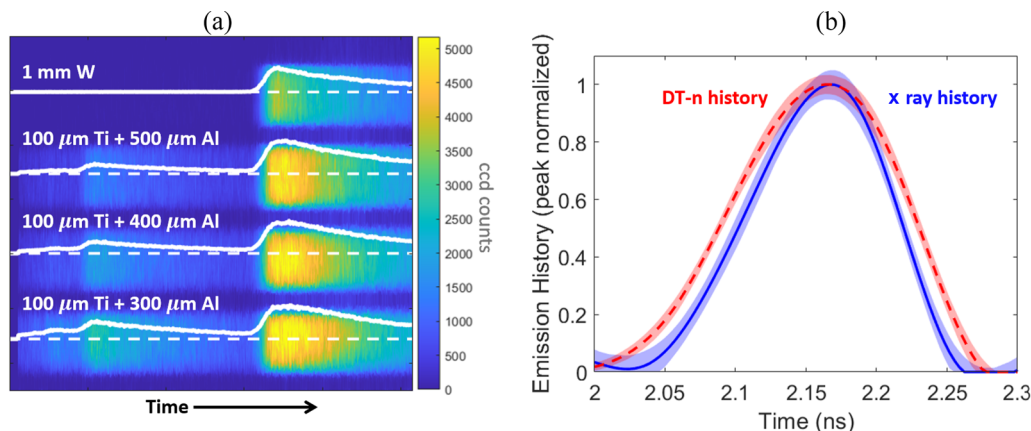
FIG. 5. (a) Phase-2 PXTD streak image collected for OMEGA DT gas-filled Cryo surrogate implosion 100521. (b) The deconvolved x-ray emission history (blue) and DTn emission history (red) determined by summing the relevant channels in (a) and then deconvolving the IRF. The shaded regions are the 95% confidence intervals. With this measurement, it is determined that the x-ray and DTn bang times are consistent with being simultaneous within the 10 ps uncertainty. A diagram of the imploded capsule is also shown.

gas-filled shock-driven implosions at OMEGA. Figure 6(a) shows a phase-2 PXTD streak image for the warm OMEGA shock driven implosion 101922. In this case, the 1-mm tungsten channel is blank because the DDn yield is not large enough to measure. The other three channels captured both x rays and D^3Hep, which are summed, and the IRF is deconvolved to determine the emission histories shown in Fig. 6(b). In this experiment, the D^3Hep bang time significantly proceeds the x-ray bang time, and both occur while the laser is still on. In this case, it is difficult to determine if the x-ray emission is primarily coming from the core or corona.

V. FUTURE UPGRADE FOR USE ON OMEGA CRYO-DT EXPERIMENTS

As discussed in Ref. 13, the current system does not have the dynamic range to simultaneously and accurately capture the DTn

and x-ray emission histories produced by a Cryo-DT implosion. The reason for this is that the DTn signal is significantly brighter than the core x rays, and the DTns cannot be attenuated before their arrival at the scintillators. The scintillator emission can be ND filtered by a factor of 20X to capture the DTn signal, but the x-ray statistics will be poor. On the other hand with no ND filtering, the x-ray emission can be captured, but the DTn signal will saturate the camera. A future phase-3 upgrade has been proposed to utilize two independent streak cameras. The newly implemented PXTD streak camera will be triggered earlier to capture the x-ray emission histories, and not the DTn, to avoid saturation effects. The upgrade to the back-end is depicted in Fig. 7. A partial reflector will be inserted in the optical path to divert a fraction of the incident scintillator light into a new relay and PXTD streak camera. Within this new relay, neutral density filters will be positioned in an intermediate image plane, which will allow per-channel ND filtering that can be adjusted
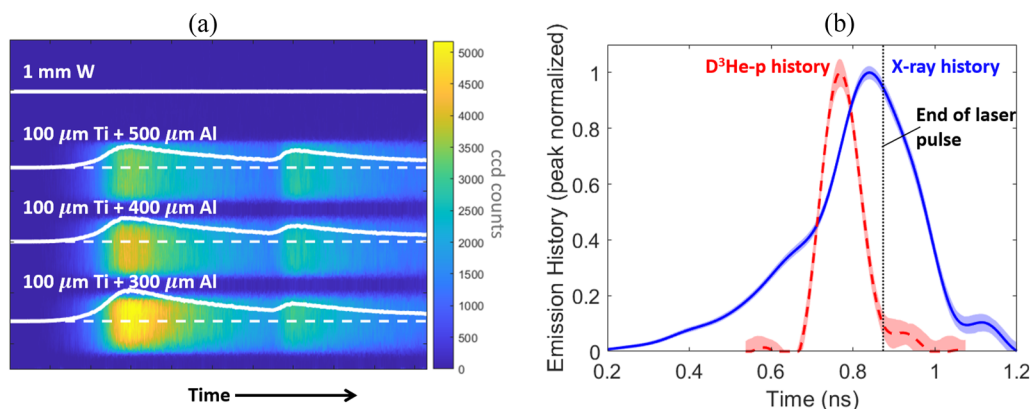

FIG. 6. (a) Phase-2 PXTD streak image for OMEGA D^3He gas-filled shock-driven implosion 101922. (b) The deconvolved x-ray emission history (blue) and D^3Hep emission history (red) determined from the sum of the relevant channels in (a). The shaded regions are the 95% confidence intervals. For this implosion, the peak of the x-ray emission occurs while the laser is still on making it difficult to distinguish between core and coronal/LPI emissions. A diagram of the imploded capsule is shown.
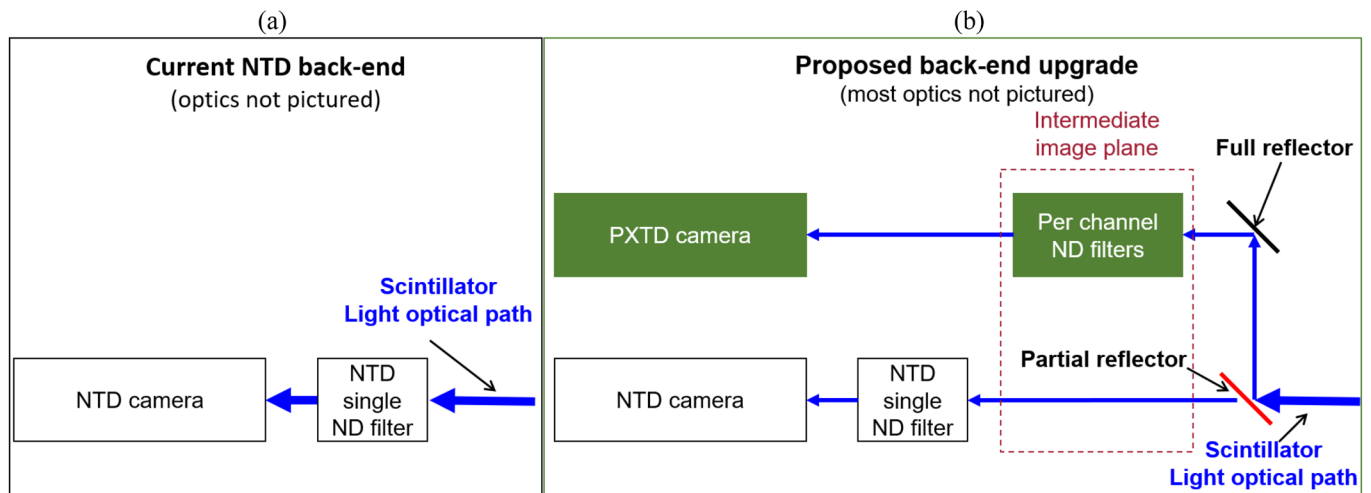
FIG. 7. (a) A simplified schematic of the scintillator light path for the phase-2 PXTD through the neutral density filtering and into an optical streak camera. (b) Simplified schematic of the proposed phase-3 PXTD, which will utilize two independent streak cameras for simultaneous high-accuracy measurements of x ray, DTn, and T_e histories from OMEGA Cryo-DT experiments. Using a partial reflector, a portion of the scintillator emission will be directed through per-channel neutral density filters located in an intermediate image plane and into a new optical streak camera.

during an experimental shot day. This is a substantial improvement over the current system of including ND filtering within the nosecone, which cannot be adjusted without venting the target chamber. With the phase-3 configuration, high quality x-ray emission histories will be recorded on the PXTD streak camera without impacting the DTn history measurement on the NTD streak camera. In addition to back end improvements, the nosecone filtering will be redesigned to include a five x-ray channel setup for a more accurate determination of $T_e(t)$.

VI. CONCLUSIONS

The phase-2 PXTD has been implemented for the measurement of $T_e(t)$ with 40 ps time resolution and <10% uncertainty at peak emission on warm OMEGA implosions. The instrument has also been used to simultaneously capture x-ray and nuclear emission histories with 10 ps relative timing uncertainty. Plans are in place to upgrade the system to "Phase-3" for measurement of $T_e(t)$ on OMEGA Cryo-DT experiments. This diagnostic is ready for use in a variety of experiments at OMEGA.

ACKNOWLEDGMENTS

AUTHOR DECLARATIONS

Conflict of Interest

The authors have no conflicts to disclose.

Author Contributions

N. Kabadi: Data curation (equal); Formal analysis (equal); Investigation (equal); Methodology (equal); Supervision (equal); Writing – original draft (equal). **P. Adrian**: Investigation (equal). **C. Stoeckl**: Investigation (equal). **A. Sorce**: Project administration (equal). **H. W. Sio**: Conceptualization (equal). **M. Bedzyk**: Methodology (equal). **T. Evans**: Methodology (equal). **S. Ivancic**: Project administration (equal). **J. Katz**: Investigation (equal). **J. Knauer**: Investigation (equal). **J. Pearcy**: Investigation (equal). **D. Weiner**: Project administration (equal). **R. Betti**: Investigation (equal). **A. Birkel**: Resources (equal). **D. Cao**: Software (equal). **M. Gatu Johnson**: Project administration (equal). **S. P. Regan**: Project administration (equal). **R. D. Petrasso**: Funding acquisition (equal); Project administration (equal). **J. Frenje**: Funding acquisition (equal); Project administration (equal).

DATA AVAILABILITY

The data that support the findings of this study are available from the corresponding author upon reasonable request.

REFERENCES

[1] R. S. Craxton, K. S. Anderson, T. R. Boehly, V. N. Goncharov, D. R. Harding, J. P. Knauer, R. L. McCrory, P. W. McKenty, D. D. Meyerhofer, J. F. Myatt, A. J. Schmitt, J. D. Sethian, R. W. Short, S. Skupsky, W. Theobald, W. L. Kruer, K. Tanaka, R. Betti, T. J. B. Collins, J. A. Delettrez, S. X. Hu, J. A. Marozas, A. V. Maximov, D. T. Michel, P. B. Radha, S. P. Regan, T. C. Sangster, W. Seka, A. A. Solodov, J. M. Soures, C. Stoeckl, and J. D. Zuegel, "Direct-drive inertial confinement fusion: A review," Phys. Plasmas 22(11), 110501 (2015).

[2] J. D. Lindl, A. Peter, R. L. Berger, S. Gail Glendinning, S. H. Glenzer, S. W. Haan, R. L. Kauffman, O. L. Landen, and L. J. Suter, "The physics basis for ignition using indirect-drive targets on the National Ignition Facility," Phys. Plasmas 11(2), 339–491 (2004).

[3] V. Y. Glebov, C. Stoeckl, T. C. Sangster, S. Roberts, G. J. Schmid, R. A. Lerche, and M. J. Moran, "Prototypes of National Ignition Facility neutron time-of-flight detectors tested on OMEGA," Rev. Sci. Instrum. 75(10), 3559–3562 (2004).

[4] T. J. Murphy, "The effect of turbulent kinetic energy on inferred ion temperature from neutron spectra," Phys. Plasmas 21(7), 072701 (2014).

[5] M. Gatu Johnson, B. D. Appelbe, J. P. Chittenden, A. Crilly, J. Delettrez, C. Forrest, J. A. Frenje, V. Y. Glebov, W. Grimble, B. M. Haines, I. V. Igumenshchev, R. Janezic, J. P. Knauer, B. Lahmann, F. J. Marshall, T. Michel, F. H. Séguin, C. Stoeckl, C. Walsh, A. B. Zylstra, and R. D. Petrasso, "Impact of imposed mode 2 laser drive asymmetry on inertial confinement fusion implosions," Phys. Plasmas 26(1), 012706 (2017).

[6] K. M. Woo, R. Betti, O. M. Mannion, C. J. Forrest, J. P. Knauer, V. N. Goncharov, P. B. Radha, D. Patel, V. Gopalaswamy, and V. Y. Glebov, "Inferring thermal ion temperature and residual kinetic energy from nuclear measurements in inertial confinement fusion implosions," Phys. Plasmas 27, 062702 (2020).

[7] O. M. Mannion, A. J. Crilly, J. Frenje, V. Y. Glebov, M. Gatu Johnson, J. P. Knauer, Z. L. Mohamed, S. P. Regan, H. G. Rinderknecht, M. H. Romanofsky, C. Stoeckl, W. Theobald, and K. M. Woo, "Diagnosing the 3-D asymmetries in laser-direct-drive implosions on OMEGA," in Proceedings of the 23rd Topical Conference on High Temperature Plasma Diagnostics, December 2020.

[8] D. Cao, R. C. Shah, S. P. Regan, R. Epstein, I. V. Igumenshchev, V. Gopalaswamy, A. R. Christopherson, W. Theobald, P. B. Radha, and V. N. Goncharov, "Interpreting the electron temperature inferred from X-ray continuum emission for direct-drive inertial confinement fusion implosions on OMEGA," Phys. Plasmas 26(8), 082709 (2019).

[9] H. Sio, J. A. Frenje, J. Katz, C. Stoeckl, D. Weiner, M. Bedzyk, V. Glebov, C. Sorce, M. Gatu Johnson, H. G. Rinderknecht, A. B. Zylstra, T. C. Sangster, S. P. Regan, T. Kwan, A. Le, A. N. Simakov, W. T. Taitano, L. Chacòn, B. Keenan, R. Shah, G. Sutcliffe, and R. D. Petrasso, "A Particle X-ray Temporal Diagnostic (PXTD) for studies of kinetic, multi-ion effects, and ion-electron equilibration rates in Inertial Confinement Fusion plasmas at OMEGA (invited)," Rev. Sci. Instrum. 87(11), 11D701 (2016).

[10] C. Stoeckl, R. Boni, F. Ehrne, C. J. Forrest, V. Y. Glebov, J. Katz, D. J. Lonobile, J. Magoon, S. P. Regan, M. J. Shoup, A. Sorce, C. Sorce, T. C. Sangster, and D. Weiner, "Neutron temporal diagnostic for high-yield deuterium–tritium cryogenic implosions on OMEGA," Rev. Sci. Instrum. 87(5), 053501 (2016).

[11] R. A. Lerche and D. W. Phillon, "Rise time of BC-422 plastic scintillator <20 ps," in Conference Record of the 1991 IEEE Nuclear Science Symposium and Medical Imaging Conference (IEEE, 1992), Vol. 1, pp. 167–170.

[12] R. A. Lerche, J. W. McDonald, R. L. Griffith, G. V. de Dios, D. S. Andrews, A. W. Huey, P. M. Bell, O. L. Landen, P. A. Jaanimagi, and R. Boni, "Preliminary performance measurements for a streak camera with a large-format direct-coupled charge-coupled device readout," Rev. Sci. Instrum. 75, 4042–4044 (2004).

[13] N. Kabadi, A. Sorce, C. Stoeckl, H. W. Sio, P. Adrian, M. Bedzyk, J. Frenje, J. Katz, J. Knauer, J. Pearcy, D. Weiner, B. A. Aguirre, R. Betti, A. Birkel, D. Cao, M. Gatu Johnson, D. Patel, R. D. Petrasso, and S. P. Regan, "A multi-channel X-ray temporal diagnostic for measurement of time-resolved electron temperature in cryogenic deuterium–tritium implosions at OMEGA," Rev. Sci. Instrum. 92(2), 023507 (2021).

[14] S. Ghosh, R. Boni, and P. A. Jaanimagia, "Optical and X-ray streak camera gain measurements," Rev. Sci. Instrum. 75, 4042–4044 (2004).

[15] H. Akima, "A method of bivariate interpolation and smooth surface fitting for irregularly distributed data points," ACM Trans. Math. Software 4(2), 148–159 (1978).

[16] R. A. Lerche and T. J. Ognibene, "Error analysis for fast scintillator-based inertial confinement fusion burn history measurements," Rev. Sci. Instrum. 70(1), 1217–1219 (1999).

[17] J. Pearcy, N. Kabadi, A. Birkel, P. Adrian, B. Lahmann, B. Reichelt, T. M. Johnson, G. Sutcliffe, J. Kunimune, M. Gatu-Johnson, A. Bose, and C. K. Li, "Characterizing X-ray transmission through filters used in high energy density physics diagnostics," Rev. Sci. Instrum. 92, 063502 (2021).

[18] P. J. Adrian et al., "X-ray-imaging spectrometer (XRIS) for studies of residual kinetic energy and low-mode asymmetries in inertial confinement fusion implosions at OMEGA," Rev. Sci. Instrum. (to be published) (2022).

[19] J. Delettrez, R. Epstein, M. C. Richardson, P. A. Jaanimagi, and B. L. Henke, "Effect of laser illumination nonuniformity on the analysis of time-resolved X-ray measurements in UV spherical transport experiments," Phys. Rev. A 36(8), 3926–3934 (1987).